Band diagrams of Si and Ge quantum wells via the 30-band k·p method

Soline Richard, Frédéric Aniel, and Guy Fishman
Institut d'Électronique Fondamentale, UMR 8622 CNRS, Bâtiment 220, Université Paris Sud, 91405 Orsay Cedex, France
(Received 26 April 2005; revised manuscript received 20 July 2005; published 12 December 2005)

We report on a method to calculate the band diagram of quantum wells using a 30-band **k·p** Hamiltonian. The subbands are calculated over the entire Brillouin zone. Such an approach is useful not only for a valence band description but also for a conduction band description when the energy minimum is not located at the center of the Brillouin zone as is the case for Si, SiGe, and Ge. The method also provides information about confinement in *L* or *X* valleys for III-V heterostructures. Such a formalism is useful for both optical calculation and for transport modeling. As an illustration, the scattering rates for holes confined in a quantum well are calculated. The accurate density of states provided by the 30-band **k·p** method gives access to very different scattering rates as compared with those obtained following an effective mass approach.

DOI: 10.1103/PhysRevB.72.245316 PACS number(s): 73.21.Fg, 73.50.Bk, 73.63.Hs

I. INTRODUCTION

The quality of modulation doped tensilely strained Si quantum wells (QW) and compressively strained Ge quantum wells both grown on relaxed SiGe virtual substrates has improved in such a way that high-mobility two-dimensional (2D) electron and hole gases can be realized. Three-dimensional (3D) full band transport models exist for SiGe alloys[1] but an effective mass method is often used to model 2D transport in SiGe layers even in the valence band[2] although hole QW electronic structures are strongly different from parabolic bands.[3] Scattering rates strongly depend on subband densities of states which are no more constant if a full band model is considered.

Several methods give access to the subbands in QW. For example, Tserbak *et al.*[4] use a tight binding model to obtain the electronic structure of strained Si/Ge superlattices in the whole Brillouin zone. The eight-band **k·p** method is often used within the envelope function formalism to obtain the confined levels in the valence band or in the Γ valley of the conduction band,[5] whereas for indirect band gap semiconductors (Si, SiGe, etc.,), confined levels in the conduction band are obtained by the effective mass approach. Moreover, when carrier heating takes place, the knowledge of the subband bottom is not sufficient. A realistic description of the $E(k)$ relation in subbands is required. Recently, we have developed a 30-band **k·p** method which gives access to the band structure of Si, Ge, and GaAs on the whole Brillouin zone with a very good accuracy on the effective masses and on the Luttinger parameters.[6] Band diagrams of bulk and strained SiGe alloys have also been calculated. The 30-band **k·p** method also allows us to calculate evanescent states in the band gap of zinc-blend-type semiconductors.[7,8]

The aim of this paper is to present an envelope function formalism based on this 30-band **k·p** method which allows us to calculate the subband structure of both electron and hole quantum wells even for indirect band gap semiconductors. This paper is organized as follows: Sec. II presents the 30-band **k·p** formalism associated with the envelope function formalism. Section III presents the electron subband structure and the envelope functions in a strained $Si/Si_{0.5}Ge_{0.5}$ quantum well. The results obtained with the 30-band **k·p** method are compared to those obtained following an effective mass approximation. In Sec. IV, the hole subband structure is calculated in a strained $Ge/Si_{0.5}Ge_{0.5}$ quantum well. The hole density of states calculated with this method is very different from the density obtained by an effective mass approach. This difference has strong consequences on scattering rates used for hole transport which are presented at the end of this part.

II. THE 30-BAND k·p FORMALISM IN SiGe HETEROSTRUCTURES

A. The 30-band Hamiltonian

To obtain strained Ge and Si band diagrams, the initial step is the band-structure calculation of bulk semiconductors using the **k·p** theory. For this purpose, we use a 30-band **k·p** Hamiltonian H_{kp} taking into account the spin-orbit coupling. H_{kp} was shown to be valid up to 5 eV above and 6 eV under the top of the valence band all over the Brillouin zone for both direct and indirect band gap semiconductors.[6] The basis functions are the same Bloch functions as the ones used by Cardona and Pollak[9] to describe Si and Ge band structures without spin-orbit coupling. We have introduced spin-orbit interaction for several reasons. It cannot be neglected for Ge in which the spin-orbit splitting is larger than 20% of the band gap energy. For Si, even if the spin-orbit splitting may be neglected to draw the band diagram ($\Delta_{so}=44$ meV$\langle\langle E_G=1.17$ eV), taking it into account gives access to explicit expressions of the Luttinger parameters.

To build $Si_{1-x}Ge_x$ band diagrams, most of the $k=0$ energy levels and the **k·p** matrix elements are linear combinations of the ones of Si and Ge. Only the energy level corresponding to the indirect gap has to follow a parabolic dispersion relation to obtain the experimental band gap variation as reported by People.[10] Unlike Si and Ge, $Si_{1-x}Ge_x$ has no inversion center. This lack of inversion center introduces a new matrix element coupling the two lower conduction bands and a new spin-orbit coupling between *p*-type valence and conduction bands. These couplings create a splitting at [100]

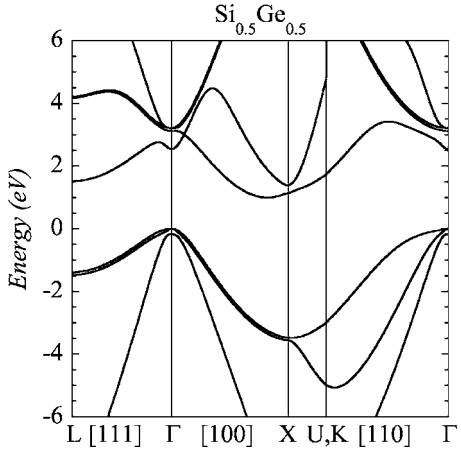

FIG. 1. Band-structure of bulk $Si_{0.5}Ge_{0.5}$ calculated with the 30-band $\mathbf{k}\cdot\mathbf{p}$ method.

point as shown in Fig. 1 for $Si_{0.5}Ge_{0.5}$ (Ref. 11). The valence band parameters A, B, C obtained in our calculation follow the same variations as those obtained by Schäffler,[12] thus demonstrating the validity of our calculation.

To solve the electronic Schrödinger equation in strained Si and Ge on $Si_{1-x}Ge_x$ with a biaxial [001] strain, we use the total Hamiltonian $H=H_{kp}+H_{st}$ where H_{st} is the strain Bir-Pikus Hamiltonian. The [001]-biaxial strain has two contributions on the band structure, a hydrostatic stress, which causes a band gap energy shift, and a uniaxial stress which produces an additional splitting of the degenerate levels by lowering the lattice symmetry. H_{st} is connected to the deformation tensor using three hydrostatic and two uniaxial potentials.[13]

Strain has strong consequences on the band diagram particularly in the valence band. It lifts the degeneracy between heavy holes (HH) and light holes (LH) at the center of the Brillouin zone. In compressively strained Ge, LH are lowered as compared to HH whereas in tensilely strained Si, HH are lowered as compared to LH. In the conduction band, strain splits the four equivalent in-plane valleys Δ_4 and the two valleys along the growth direction Δ_2. All the L valleys remain equivalent.

B. The envelope function algorithm

1. Envelope function calculation

We consider a square QW which constitutes a type I heterostructure as shown in Fig. 2. The growth direction will be taken as the z axis. In the A and B layers of the heterostructure, the wave functions ψ can be developed on the same Bloch function basis $u_{l,k_0}(r)$ (Ref. 5)

$$\psi_B(r)=\psi_B(\rho,z)=\sum_l \exp(ik_\rho\rho)\chi_l^{(B)}(z)u_{l,k_0}(r) \qquad (1)$$

in the barrier layer and

$$\psi_A(r)=\psi_A(\rho,z)=\sum_l \exp(ik_\rho\rho)\chi_l^{(A)}(z)u_{l,k_0}(r) \qquad (2)$$

in the well layer, where $\chi_l^{(A,B)}(z)$ is the envelope function. It is supposed to be continuous between the barrier and the well, at $z=a+A$ and $z=A-a$. The quantum well problem was tackled in the 30×30 $\mathbf{k}\cdot\mathbf{p}$ model in Ref. 14 with a different approximation on the Bloch functions. In Ref. 14 the authors do not take $\langle u^B_{l,k_0}|u^A_{l,k_0}\rangle=\delta_{l,m}$ but use a unitary transformation which allows one to know one set of functions (u^B_{l,k_0} in B) from the first one (u^A_{l,k_0} in A).

These wave functions still obey the Schrödinger equation but can no longer be factorized by $\exp(ikr)$, as is usually done using the "bulk" $\mathbf{k}\cdot\mathbf{p}$ method which consists of projecting the wave function ψ on the Bloch functions $u_l(r)$ at $k=0$. Consequently, the k_z wave vector is replaced by $-i(\partial/\partial z)$ in the 30-band $\mathbf{k}\cdot\mathbf{p}$ Hamiltonian. The envelope function $\chi(z)$ verifies the following equation:

$$H_{l,m}\chi(z)=\left\{\left[V(z)+\frac{\hbar^2}{2m_0}\left(k_\rho^2-\frac{d^2}{dz^2}\right)\right]\langle u_l|u_m\rangle+\frac{\hbar k_\rho}{m_0}\langle u_l|p_\rho|u_m\rangle-\frac{i\hbar}{m_0}\langle u_l|p_z|u_m\rangle\frac{d}{dz}\right\}\chi(z)=\varepsilon\chi(z), \qquad (3)$$

where $H_{l,m}$ is the 30-band $\mathbf{k}\cdot\mathbf{p}$ Hamiltonian element on line l and column m and $p_\rho=(p_x,p_y)V(z)$ corresponds to the energy shifts added on diagonal terms due to the heterostructure between the A and B layers. More precisely, Eq. (3) describes the upper part (above the diagonal) of the matrix we have used to calculate the eigenenergies. For the lower part (below the diagonal) we have taken the Hermitic conjugate, as quoted in Ref. 15. From a numerical viewpoint, once the upper part is calculated, it is enough to take the complex conjugate in the lower part to get the whole matrix.

To solve this equation, the envelope function $\chi(z)$ is calculated on the interval $[0, 2A]$ with $a\ll A$, so as to obtain $\chi(0)=\chi(2A)=0$. It is projected on a test function basis $\varphi_j(z)$

$$\chi(z)=\sum_j a_j\varphi_j(z) \quad \text{with } \varphi_j(0)=\varphi_j(2A)=0.$$

The aim of the calculation is to obtain the a_j coefficients, eigenvector components of the Hamiltonian developed on a test function basis $\varphi_j(z)$. The eigenvalues give the energy levels. To evaluate the envelope function, each element $H_{l,m}$ of the 30-band $\mathbf{k}\cdot\mathbf{p}$ Hamiltonian is written as an auxiliary square matrix containing N^2 elements, where N is the $\varphi_j(z)$ function basis dimension. A $30\times N$ square matrix has to be diagonalized to obtain the envelope function.

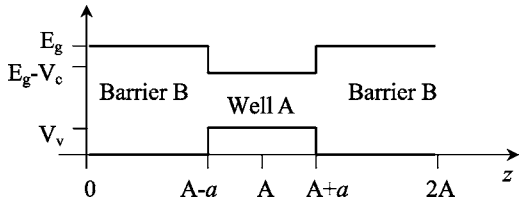

FIG. 2. Band edge profile of a type I heterostructure. E_G is the band gap of the barrier and E_G-V_c-V_v is the band gap of the well.

2. Test functions

Choosing test functions depends on the k-space location where the subbands are calculated. In the Γ valley, for holes

or electrons in direct gap semiconductors, the usual functions are the following:

$$\chi(z) = \sum_j a_j \varphi_j(z) = \sum_j a_j \left[\frac{1}{\sqrt{A}} \sin\left(\frac{j\pi z}{2A} \right) \right]. \quad (4)$$

Around Γ, this basis gives access to the subbands with $N < 50$ as shown in Ref. 3, but it does not allow us to obtain the subband elsewhere in the Brillouin zone, for instance in an L or a Δ valley. Indeed, in silicon, to access a Δ_2 valley centered at k_{ez}, N has to verify

$$\frac{N\pi}{2A} > k_{ez} = 0.85 \frac{2\pi}{a_0}, \text{ i.e., } N > 0.85 \frac{4A}{a_0}.$$

where a_0 is the lattice parameter. Considering a 5-nm-wide QW, with $A = 30$ nm, these test functions give $N > 180$. It explains why the following test functions are chosen to obtain the subbands in a valley centered at $k_e = (k_{ex}, k_{ey}, k_{ez})$:

$$\varphi_n(z) = \frac{\exp(ik_{ez}z)}{\sqrt{A}} \sin\left(\frac{n\pi z}{2A} \right). \quad (5)$$

With these test functions, the Hamiltonian term on line $j + N \times (l-1)$ and column $g + N \times (m-1)$ is written

$$\langle \varphi_j | H_{l,m} | \varphi_g \rangle = \int_0^{2A} \left[\frac{\exp(-ik_{ez}z)}{\sqrt{A}} \sin\left(\frac{j\pi z}{2A} \right) \right] \times H_{l,m} \left[\frac{\exp(ik_{ez}z)}{\sqrt{A}} \sin\left(\frac{g\pi z}{2A} \right) \right] dz. \quad (6)$$

The subbands of the QW are obtained by diagonalizing this $30N \times 30N$ Hamiltonian. To perform this calculation with a good accuracy (less than 1 meV uncertainty), $N = 40$ is a typical value allowing a good compromise between CPU time and precision. The test function of Eq. (5) allows one to calculate the subband dispersion relation everywhere in the Brillouin zone at a fixed k_{ez} point. This point often corresponds to a valley point where carriers can be confined, for example, at a Δ point in Si or an L point in Ge. The following sections present two different examples concerning electrons in the Δ valley of tensilely strained silicon on $Si_{0.5}Ge_{0.5}$, and holes in the Γ valley of compressively strained germanium on $Si_{0.5}Ge_{0.5}$. The same method is used for both electrons and holes. The only difference is the value of k_{ez} for electrons, $k_{ez} = 0.85(2\pi/a_0)$ whereas for holes $k_{ez} = 0$.

III. STRAINED Si ON $Si_{0.5}Ge_{0.5}$ ELECTRONS IN QUANTUM WELLS

The electron subbands are calculated within the 30-band method and are compared to those obtained within the effective mass approximation in a square 5-nm-thick QW. In silicon, strain lowers the Δ valleys in the growth direction Δ_2 as compared to those in the layer plane Δ_4. Electrons in Δ_4 valley are not confined as shown in Fig. 3. Strained silicon on $Si_{0.5}Ge_{0.5}$ creates a type II heterojunction since the holes are not confined in the silicon layer.

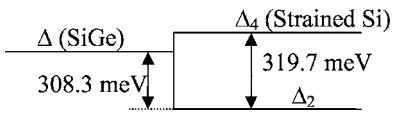

FIG. 3. Conduction band edge profile of strained Si on $Si_{0.5}Ge_{0.5}$.

TABLE I. Effective masses and confinement potential in the strained Si QW on $Si_{0.5}Ge_{0.5}$.

	Δ_2 valley
Confinement potential	308.3 meV
Longitudinal effective mass in the barrier m_B	0.947
Longitudinal effective mass in the well m_A	0.925

We first recall the effective mass approach. Both well and barrier materials have a Δ valley. The corresponding effective masses calculated from the band diagrams obtained within the 30-band $\mathbf{k}\cdot\mathbf{p}$ method are recalled in Table I. The BenDaniel-Duke Hamiltonian we have to solve is the following:[16]

$$\left(p_z \frac{1}{2m(z)} p_z + V(z) \right) \chi(z) = E\chi(z). \quad (7)$$

The energy reference has been taken at the bottom of the Δ_2 valley. $m(z)$ is the longitudinal effective mass in strained Si in the well and in $Si_{0.5}Ge_{0.5}$ in the barrier. The envelope function is sinusoidal in the well and decreases exponentially in the barrier. As recalled by Bastard and Brum,[5] the energy levels verify $E = \hbar^2 k^2 / 2m_A = V_P - \hbar^2 K^2 / 2m_B$ where k is the wave vector in the well and K the decreasing coefficient in the barrier. k verifies

$$ka \tan ka = \sqrt{\frac{m_A}{m_B}} \sqrt{\frac{V_P}{(\hbar^2/2m_A a^2)} - (ka)^2} \text{ or}$$
$$-ka \operatorname{cotan} ka = \sqrt{\frac{m_A}{m_B}} \sqrt{\frac{V_P}{(\hbar^2/2m_A a^2)} - (ka)^2}. \quad (8)$$

To obtain electron subbands in a 5-nm-thick square Ge QW via the 30-band $\mathbf{k}\cdot\mathbf{p}$ method, the basis of test functions is the following:

TABLE II. Subband energy levels in the strained Si QW on $Si_{0.5}Ge_{0.5}$, calculated with the $\mathbf{k}\cdot\mathbf{p}$ method and with an effective mass approach.

Subband	Effective mass	30-band $\mathbf{k}\cdot\mathbf{p}$
$E1$(meV)	12.23	13.10
$E2$(meV)	48.70	49.19
$E3$(meV)	108.4	108.2
$E4$(meV)	189.2	187.8

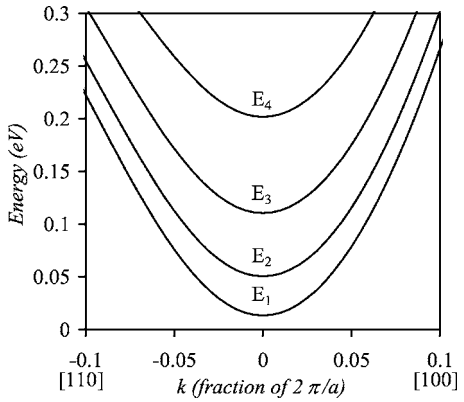

FIG. 4. Strained Si 5-nm-thick QW on $Si_{0.5}Ge_{0.5}$: dispersion of the electron subbands in [100] and [110] directions of the k space calculated via the $\mathbf{k}\cdot\mathbf{p}$ 30-band method. The $k=0$ point corresponds to the minimum of a Δ_2 valley. From bottom to top, the subbands correspond to the E_1, E_2, E_3, and E_4 subbands.

$$\varphi_n(z) = \frac{\exp(ik_{ez}z)}{\sqrt{A}}\sin\left(\frac{n\pi z}{2A}\right) \text{ with } k_{ez} = 0.85\frac{2\pi}{a_0}. \quad (9)$$

Table II shows a comparison between confined levels obtained within the $\mathbf{k}\cdot\mathbf{p}$ method and the effective mass approach. The small discrepancy (less than 1 meV) between the energy levels calculated by the two methods shows the reliability of the 30-band $\mathbf{k}\cdot\mathbf{p}$ method associated with the envelope function formalism even at the Δ point or anywhere in the Brillouin zone.

The advantage of the $\mathbf{k}\cdot\mathbf{p}$ method is to obtain not only the subbands minima but also all the dispersion relations in the layer plane (k_x,k_y) as shown in Fig. 4. Figure 5 gives the envelope functions associated with each subband. Figure 6 represents equi-energy lines at 150 meV above the minimum of the strained silicon conduction band. Equi-energy lines are almost circles in the Si layer plane; they stem from slices of ellipsoidal equi-energy surfaces of bulk silicon in transverse direction. As opposed to the case of the valence band, the

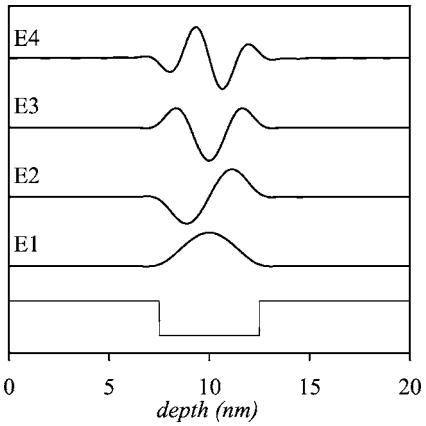

FIG. 5. Strained Si 5-nm-thick QW on $Si_{0.5}Ge_{0.5}$: envelope functions representation of the electron confined states obtained at the Δ valley minimum. The corresponding levels are from bottom to top E_1, E_2, E_3, and E_4.

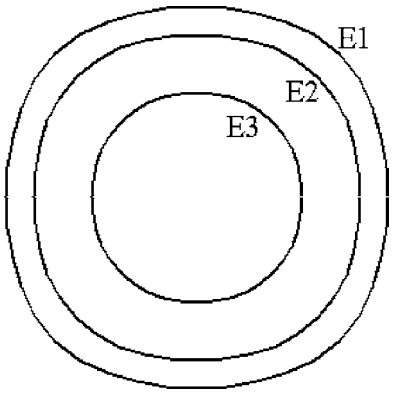

FIG. 6. Strained Si 5-nm-thick QW on $Si_{0.5}Ge_{0.5}$: equi-energy lines at 150 meV above the minimum of the conduction band. The corresponding levels are from center to edge E_3, E_2, and E_1. The E_4 energy level is larger than 150 meV.

electron subbands are parallel and have nearly the same allure as the Δ_2 valley in strained silicon. Indeed, the strong coupling between light and heavy hole bands deeply modifies the allure of the hole subbands whereas the electron subbands only stem from one band. Table III gives the effective mass as extracted from each subband, compared with the transverse effective mass of strained silicon in the Δ_2 valley. Even if the curvature of the subbands seems to be constant in Fig. 4, the corresponding effective mass increases with the energy level of the subband. The 30-band $\mathbf{k}\cdot\mathbf{p}$ model shows a variation of 4% of the effective mass which was, of course, not accounted for by the effective mass approach.

IV. STRAINED Ge ON $Si_{0.5}Ge_{0.5}$ HOLE QUANTUM WELLS

A. Band diagram and envelope functions

To obtain hole subbands in a 5-nm-thick square Ge QW, the basis of test functions is the following:

$$\varphi_n(z) = \frac{1}{\sqrt{A}}\sin\left(\frac{n\pi z}{2A}\right). \quad (10)$$

In the valence band, the barrier height is 350 meV between the top of the valence band in bulk $Si_{0.5}Ge_{0.5}$ and strained Ge. This heterojunction is type I but the conduction band barrier is almost zero (10 meV). Figure 7 shows the subbands obtained with 40 test functions along [100] and [110] directions and Fig. 8 shows the corresponding envelope functions at $k=0$. This band diagram is strongly different

TABLE III. Strained Si QW on $Si_{0.5}Ge_{0.5}$. Effective masses obtained for each electron subband. The transverse effective mass in Δ_2 valley for strained Si is $0.1812m_0$.

Subband	Effective mass
$E1(m_0)$	0.1834
$E2(m_0)$	0.1841
$E3(m_0)$	0.1852
$E4(m_0)$	0.1893

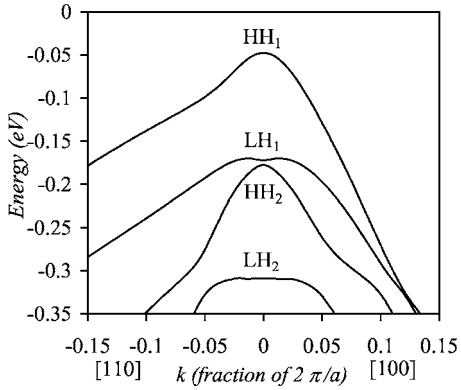

FIG. 7. Strained Ge 5-nm-thick QW on $Si_{0.5}Ge_{0.5}$: dispersion of the hole subbands in [100] and [110] directions of the k space. From top to bottom, the subbands correspond to the HH_1, LH_1, HH_2, and LH_2 subbands.

from the one obtained for the conduction band (Fig. 4) because it stems from the two HH and LH bands which are strongly coupled. Anticrossing points appear, for example, in the [100] direction between HH_1 and LH_1 subbands. Even around the Γ point, the effective mass approximation is meaningless. For example, the curvature of the LH_1 subband is negative at $k=0$. The envelope functions associated with these subbands at the Γ point are sinusoidal in the well and exponentially decreasing in the barrier. To confirm the reliability of this 30-band $\mathbf{k}\cdot\mathbf{p}$ method in the valence band, no comparison with the effective mass calculation is possible because the valence band is strongly anisotropic, even near the Γ point. That is why the results have been compared to those obtained with a 14-band method in the case of a 5-nm-thick $Si_{0.5}Ge_{0.5}$ QW on Si.[3] This 14-band $\mathbf{k}\cdot\mathbf{p}$ method has shown its efficiency to describe the electronic structure of direct band gap semiconductors along almost 30% of the Brillouin zone.[17] If the same Luttinger parameters are taken into account, both the 14-band and 30-band methods give the same subband diagrams in this SiGe hole QW. The shape of this band diagram has strong consequences on the 2D density of states in the well, as shown in Sec. IV B.

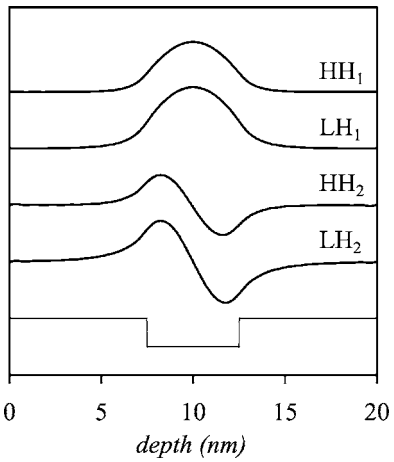

FIG. 8. Strained Ge 5-nm-thick QW on $Si_{0.5}Ge_{0.5}$: envelope functions representation of the hole confined states. The corresponding levels are from top to bottom HH_1, LH_1, HH_2, LH_2.

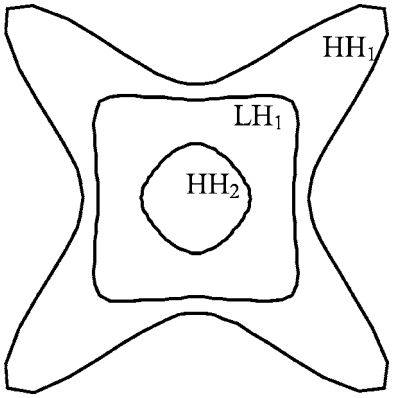

FIG. 9. Strained Ge on $Si_{0.5}Ge_{0.5}$ 5-nm-thick QW: equi-energy lines at 250 meV in the valence band. The corresponding levels are from center to edge HH_2, LH_1, and HH_1. The LH_2 energy level is larger than 250 meV.

B. Calculation of 2D density of states

In a three-dimensional semiconductor, for each band α, the density of states at energy E is defined as[18]

$$g_\alpha(E) = \int \frac{dk}{4\pi^3}\delta[E - E_\alpha(k)] = \int_{S_\alpha(E)} \frac{dS}{4\pi^3}\frac{1}{|\nabla_k(E_\alpha)|}, \tag{11}$$

where S_α(E) is the equi-energy surface in the whole Brillouin zone. In a two-dimensional layer, for each subband n, the density of states depends on the wave vector in the plane of the layer k_ρ. Its definition, deduced from the three-dimensional case, is the following:

$$g_n(E) = \int \frac{dk_\rho}{2\pi^2}\delta[E - E_n(k_\rho)] = \int_{L_n(E)} \frac{dl}{2\pi^2}\frac{1}{|\nabla_{k_\rho}(E_n)|}, \tag{12}$$

where $L_n(E)$ is the equi-energy line in the Brillouin zone. Figure 9 shows the shape of equi-energy lines at 250 meV in the Ge QW. From a numerical point of view, one needs to approximate these equi-energy lines to calculate densities of states. The Brillouin zone is divided in squares at the center of which the energy of each subband is calculated and tabulated. An algorithm derived from the one introduced by Gilat and Raubenheimer[19] is used to define an approximate equi-energy line at the desired energy within each square.

Figure 10 shows the 2D density of states in the germanium QW studied above. This density of states is constant for each subband in the effective mass approximation whereas a full band calculation gives a very different result. The maximum obtained for the LH_1 subband is an artifact due to the numerical calculation of gradient around the point where the curvature sign changes. Except for this artifact, the density of states is far from being constant in each subband. This has strong consequences on scattering rates useful for transport calculation which are presented in Sec IV C.

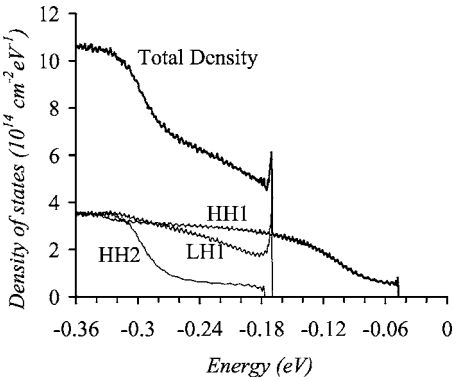

FIG. 10. Strained Ge on $Si_{0.5}Ge_{0.5}$ 5-nm-thick QW: two-dimensional hole density of states in k space.

C. Calculation of scattering rates for hole transport properties in Ge QW

To study hole transport in the undoped Ge channel of a heterojunction field effect transistor, the Boltzmann transport equation gives access to the distribution function $f(k_\rho, r, t)$ with $k_\rho = k_x e_x + k_y e_y$ in each subband taking into account electric field and phonon interactions. Scattering rates used to solve the Boltzmann transport equation are proportional to the density of states available for the final particle. For example, let us consider acoustic phonon interaction. The acoustic interaction probability is written as[20]

$$P_{ac}(k_\rho, k'_\rho) = \frac{2\pi E_{ac}^2 k_B T}{\hbar \rho s^2} \delta(\varepsilon' - \varepsilon) \int \chi_m^2(z)\chi_n^2(z)dz, \quad (13)$$

where ε, k_ρ and ε', k'_ρ are, respectively, initial and final state energies and wave vectors, s is the crystal sound velocity, ρ is the crystal density, E_{ac} is the acoustic potential in eV/m, $\chi_{m,n}(z)$ are envelope functions in initial and final subbands, k_B is the Boltzmann constant, $\hbar$ the reduced Planck constant, and δ is the Dirac function. The acoustic scattering rate is written as

$$\lambda_{ac} = \frac{1}{4\pi^2}\int_k P_{ac}(k_\rho, k'_\rho)d^2k_\rho = A\int_{L(\varepsilon)} \frac{dl}{|\nabla_{k_\rho}(\varepsilon)|}\int \chi_m^2(z)\chi_n^2(z)dz \quad (14)$$

with $A = k_B T E_{ac}^2 / 2\pi\hbar\rho s^2$ and $\varepsilon' = \varepsilon$.

The two-dimensional density of states appears in this scattering rate, multiplied by the envelope function overlap integral. A similar expression is obtained for optical phonon scattering rates, except for the fact that the phonon energy is not taken equal to zero. The optical interaction probability is written as[21]

$$P_{op}(k_\rho, k'_\rho) = \frac{\pi\hbar E_{op}^2}{\hbar\rho\omega_{op}}\left(N_{op} + \frac{1}{2} \mp \frac{1}{2}\right)\delta(\varepsilon' - \varepsilon \pm \hbar\omega_{op}) \times \int \chi_m^2(z)\chi_n^2(z)dz, \quad (15)$$

where $\hbar\omega_{op}$ is the phonon energy, E_{op} is the deformation potential and

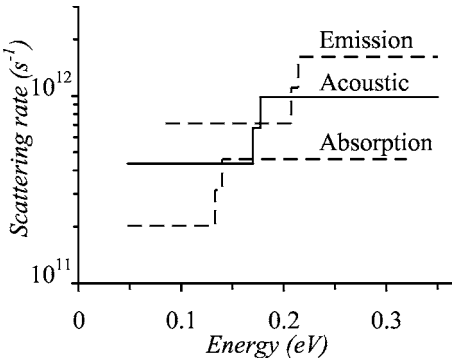

FIG. 11. Optical and acoustic phonon scattering rates for holes initially in the HH_1 subband taken into account to solve the 2D Boltzmann transport equation in the effective mass approximation. For each scattering rate, the first stair corresponds to the HH_1 intrasubband interaction, the second stair is the sum of the HH_1 intrasubband interaction plus the HH_1-LH_1, intersubband interaction, and the third stair corresponds to HH_1 intrasubband interaction plus HH_1-LH_1 and HH_1-HH_2 intersubband interactions. LH_1 and HH_2 energy levels are, respectively, 170 and 177 meV, explaining that the two last stairs are near to each other.

$$N_{op} = \frac{1}{\exp\left(\frac{\hbar\omega_{op}}{k_B T}\right) - 1}$$

is the optical phonon density. The upper sign corresponds to phonon absorption and the lower sign to phonon emission. The optical scattering rate is the following:

$$\lambda_{op} = \frac{1}{4\pi^2}\int_{k'} P_{op}(k_\rho, k'_\rho)d^2k_\rho = A\int_{L(\varepsilon')} \frac{dl}{|\nabla_{k'_\rho}(\varepsilon')|}\int \chi_m^2(z)\chi_n^2(z)dz \quad (16)$$

with $A = (\hbar E_{op}^2 / 4\pi\rho\hbar\omega_{op})(N_{op} + \frac{1}{2} \mp \frac{1}{2})$ and $\varepsilon' = \varepsilon \pm \hbar\omega_{op}$.

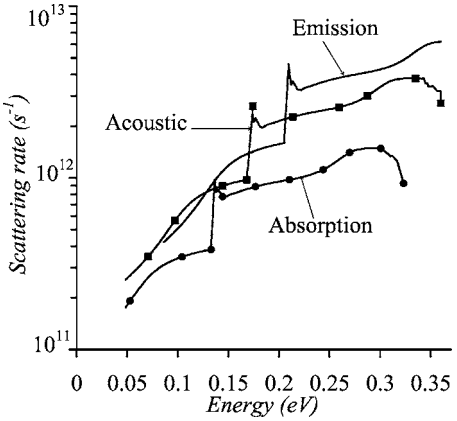

FIG. 12. Optical and acoustic phonon scattering rates for holes initially in the HH_1 subband taken into account to solve the 2D Boltzmann transport equation, calculated using the real subband dispersion relation. These interaction rates no longer look like stairs: the corresponding density of states is not constant for each subband if the real dispersion relation is taken into account.

In the effective mass approach, the density of states is constant for each subband so the scattering rates have a staircase shape[22] whereas taking into account the density of states which stems from the real subband structure gives varying scattering rates. Figure 11 shows the optical and acoustic phonon scattering rates for holes in the first subband (HH_1) calculated in the effective mass approach and Fig. 12 shows the same rates calculated with the real density of states. This difference between scattering rates may have strong consequences on hole mobility in the Ge QW.

V. CONCLUSION

We have presented how the 30-band $\mathbf{k}\cdot\mathbf{p}$ method associated with an envelope function formalism allows us not only to calculate the subbands in the Brillouin zone center but everywhere in the Brillouin zone. The 30-band $\mathbf{k}\cdot\mathbf{p}$ method gives us access to bulk and strained SiGe alloys band diagrams all over the Brillouin zone, whatever the Ge content. Associated with the $\mathbf{k}\cdot\mathbf{p}$ method, the envelope function formalism uses test functions which are usually sinusoids to obtain subbands in direct gap semiconductors.[3] In this paper, the same formalism, with slightly different test functions, is used to obtain hole and electron subbands in an indirect gap semiconductor. We have explained the choice of these new test functions and shown the efficiency of this method by calculating the subband diagram and the envelope functions in a strained Si on $Si_{0.5}Ge_{0.5}$ electron QW. The energy levels in the Δ point are almost the same as those obtained using an effective mass approximation, but this method also gives access to the real shape of the subbands, unlike the effective mass approach. Hole subbands are calculated in a strained Ge on $Si_{0.5}Ge_{0.5}$ QW, with the same method. The hole subband structure allows us to calculate the two-dimensional real density of states and gives access to two-dimensional "full band" scattering rates needed for accurate transport simulation.

ACKNOWLEDGMENT

We thank Philippe Boucaud for a careful reading of the manuscript.

[1] M. V. Fischetti and S. E. Laux, Phys. Rev. B **38**, 9721 (1988).
[2] G. C. Crow and R. A. Abram, Solid State Technol. **15**, 7 (2000).
[3] M. Elkurdi, G. Fishman, S. Sauvage, and P. Boucaud, Phys. Rev. B **68**, 165333 (2003).
[4] C. Tserbak, H. M. Polatoglou, and G. Theodorou, Phys. Rev. B **47**, 7104 (1993).
[5] G. Bastard and J. A. Brum, IEEE J. Quantum Electron. **22**, 1625 (1986).
[6] S. Richard, F. Aniel, and G. Fishman, Phys. Rev. B **70**, 235204 (2004).
[7] S. Richard, H.-J. Drouhin, N. Rougemaille, and G. Fishman, J. Appl. Phys. **97**, 083706 (2005).
[8] N. Rougemaille, H.-J. Drouhin, S. Richard, G. Fishman, and A. K. Schmid, Phys. Rev. Lett. **95**, 186406 (2005).
[9] M. Cardona and F. Pollak, Phys. Rev. **142**, 530 (1966).
[10] R. People, Phys. Rev. B **32**, 1405 (1985).
[11] U. Schmid, N. E. Christensen, and M. Cardona, Phys. Rev. B **41**, 5919 (1990).
[12] F. Schäffler, Semicond. Sci. Technol. **12**, 1515 (1997).
[13] S. Richard, N. Cavassilas, F. Aniel, and G. Fishman, J. Appl. Phys. **94**, 1795 (2003).
[14] L. Wang Wang and A. Zunger, Phys. Rev. B **54**, 11417 (1996).
[15] B. A. Foreman, Phys. Rev. B **56**, R12748 (1997).
[16] D. J. BenDaniel and C. B. Duke, Phys. Rev. **152**, 683 (1966).
[17] P. Pfeffer and W. Zawadzki, Phys. Rev. B **53**, 12813 (1996).
[18] N. W. Ashcroft and N. D. Mermin, *Solid State Physics* (Saunders, New York, 1976).
[19] G. Gilat and L. J. Raubenheimer, Phys. Rev. **144**, 390 (1966).
[20] T. Ando, A. B. Fowler, and F. Stern, Rev. Mod. Phys. **54**, 437 (1982).
[21] R. Oberhuber, G. Zandler, and P. Vogl, Phys. Rev. B **58**, 9941 (1998).
[22] B. K. Ridley, J. Phys. C **15**, 5899 (1982).